Desalination and Water Treatment
www.deswater.com

doi: 10.5004/dwt.2021.27013

220 (2021) 392–408
April

Comparative adsorption of anionic dye Congo red and purification of olive mill wastewater by chitin and their derivatives

Rihab Belhadj Ammar[a], Abdelkader Labidi[a,b], Asier M. Salaberria[c], Jalel Labidi[c,*], Sameh Ayadi[b], Manef Abderrabba[b]

[a]*Chemistry Department, El Manar University, University of Sciences of Tunis, B.P: 248, El Manar II, 2092, Tunis, Tunisia, emails: belhadj.rihab25@gmail.com (R.B. Ammar), abdelkaderlabidi0907@gmail.com (A. Labidi)*
[b]*Laboratory of Materials, Molecules and Applications, IPEST, Preparatory Institute of Scientific and Technical Studies of Tunis, University of Carthage, Sidi Bou Said Road, B.P. 51 2070, La Marsa, Tunisia, emails: sameh.ayadi@instm.rnrt.tn (S. Ayadi), abderrabbamanef@gmail.com (M. Abderrabba)*
[c]*Biorefinery Processes Research Group, Department of Chemical and Environmental Engineering, University of the Basque Country (UPV/EHU), Plza. Europa1, 20018 Donostia-San Sebastian, Spain, emails: jalel.labidi@ehu.es (J. Labidi), asier.martinez@ehu.es (A.M. Salaberria)*

Received 3 May 2020; Accepted 30 December 2020

ABSTRACT

In this study, chitin (CH), chitosan (CS) and epichlorohydrin cross-linked chitosan beads were applied to remove Congo red (CR) from an aqueous medium. The same materials were used for olive mill wastewater treatment as industrial reject. First, the cross-linked chitosan was synthesized by the homogeneous reaction of chitosan with epichlorohydrin in an acid solution. Then, it was characterized by attenuated total reflection–Fourier-transform infrared spectroscopy (ATR-FTIR), thermogravimetric analysis (TGA, DTGA) and scanning electron microscopy. The dye (CR) removal was analyzed by kinetics, equilibrium and thermodynamic studies. Subsequently, the three materials were tested for olive mill wastewater purification as an innovative method, which presents the originality of our work. The adsorption isotherms indicate that the Congo red adsorption was well fitted by the Langmuir isotherm equation under the studied concentrations by comparing the linear correlation to the non-linear parameters. Moreover, thermodynamic parameters showed that the adsorption was exothermic and spontaneous. The ATR-FTIR indicated the adsorption of phenolic compounds on chitosan and epichlorohydrin cross-linked chitosan was a chemical reaction. The performed experiments showed that epichlorohydrin cross-linked chitosan has high adsorption of Congo red and it can be used as potential material for olive mill wastewater treatment.

Keywords: Chitosan; Congo red; Olive mill wastewater; Epichlorohydrin; Adsorption

1. Introduction

Major water pollution can be caused by heavy metals due to rapid industrialization, urbanization and routine activities [1,2]. In our days, heavy metals are one of the inorganic compounds which present the major substrates of wastewater [3,4]. In addition to the water pollution by heavy metals, the water contamination level was increased due to the presence of organic pollutants such as dyes. Synthetic dyes are one of the major causes of water pollution. They result from discharging the wastes of textile dyeing, printing, plastics, etc. [5,6]. In fact, many dyes and pigments contain aromatic rings in their structures, which makes them toxic for human health and aquatic systems [7].

* Corresponding author.

They cannot be easily removed because of their higher resistance to bio-degradation in the aquatic medium [8]. Among them, Congo red, disodium-3,3′-([1,1′-biphenyl]-4,4′-diyl)bis(4-aminonaphthalene-1-sulfonic acid) is a benzidine-based anionic biazo dye known as a human carcinogen affecting health and environment [9]. It causes many health diseases including eye and skin problems, gastrointestinal irritation, vomiting, diarrhea and nausea to humans and animals [10] as well as a low lethal concentration (LC_{50} < 63 mg/L) of some organisms [11].

In recent years, a range of conventional treatment technologies for the removal of Congo red, such as film [12], membrane [13], photo-degradation process [14] and adsorption [15] have been extensively investigated. On the other hand, olive oil production is one of the most traditional agricultural industries with a great economic importance in most of the Mediterranean countries [16]. Tunisia is one of the first countries that release the exponentially-growing amount of olive mill wastewater (OMW) [16]. The annual production of OMW worldwide was estimated to be over 20 million m^3 [17], which represents a huge environmental problem. The OMW is characterized by the high concentrations of several organic compounds, such as organic acids, sugars, tannins and phenolic compounds (up to 10 g L^{-1}) [17] such as hydroxytyrosol which is the most abundant phenolic compound in OMW. This waste is one of the most harmful effluents produced by agro-food industries because of its high polluting load and high toxicity to the whole ecosystem (plants, aquatic organisms and air) [16,18]. In this case, technologies for the purification of OMW and the recovery of polyphenols have been developed in recent years using adsorption [19], ultrafiltration membrane [20,21] and liquid–liquid extraction [22]. The adsorption process provides an attractive alternative treatment, especially if the adsorbent is inexpensive and readily available for dye removal and OMW treatment. Chitosan, a derivative biopolymer obtained from the deacetylation of chitin, is a natural and abundant biopolymer occurring from the exoskeletons of insects, crustaceans shells and fungi cellular walls. Recently, chitosan, used as an adsorbent, has drawn the attention of scientists and researchers due to its high contents of amino and elevated nitrogen content showing high potential for the adsorption of dyes and OMW treatment resulting from its high selectivity and reactivity towards the pollutants removal [23,24]. Nonetheless, to increase chitosan's adsorbent capacity, the chemical composition of chitosan can be easily modified because of the presence of hydroxyl and amino functional groups. Chitosan derivatives are viewed as one of the most employed adsorbents for the retention of toxic dyes and OMW treatment. Numerous chitin and chitosan-based products, namely chitin-clay microspheres [25], lignin [26], chitosan–polyethylenimine [27], 2,3-dialdehyde cellulose [28] and L-monoguluronic acid [29], were prepared by graft copolymerization to enlarge this chitin and chitosan functionality and their application for dyes removal and OMW purification. Herein, cross-linked chitosan with epichlorohydrin was synthesized by a one-step method. The as-prepared powder was characterized for the adsorption of Congo red from water using adsorption kinetics and isotherms, compared to chitin and chitosan as biopolymers, after employing this chitosan derivative for OMW treatment as an industrial reject. The kinetics of phenolic compounds adsorption on chitin (CH), chitosan (CS) and chitosan–epichlorohydrin (CS-ECH) was investigated and followed by desorption studies. The results of CS-ECH were very encouraging, exhibiting high adsorption percentages of Congo red removal and olive mill wastewater purification.

2. Experimental

2.1. Materials

Chitin (CH, Fig. 1a) powder was extracted in our laboratory from yellow lobster wastes (kindly supplied by Antartic Seafood S.A., Chile). Chitosan powder (CS, Fig. 1b, degree of deacetylation of 98% and viscosity-average molecular weight of 500,000) was supplied by Mahtani Chitosan Pvt. Ltd., India. Epichlorohydrin (Sigma-Aldrich, 99%, France), acetic acid (Ph. Eur. reagent >99.5%), acetone (Sigma-Aldrich, >99%, France), sodium hydroxide (NaOH, reagent grade, ≥98%, pellets (anhydrous)), hydrochloric acid (HCl, ACS reagent, 37%), gallic acid (ACS reagent, ≥97.5%), Folin & Ciocalteu's Reagent (Sigma-Aldrich, France), sodium bicarbonates (Sigma-Aldrich, France), Congo red (Sigma-Aldrich, >85%, France). All reagents were used as received without further purification. Olive mill wastewater was collected from a unit of olive oil extraction located in Tunisia, and stored in a plastic container in a refrigerator at 4°C.

2.2. Preparation of chitosan–epichlorohydrin bead

2.0 g of chitosan powder was dissolved in 70 mL of a 1.0% aqueous solution of acetic acid under constant stirring. Then, 2.0 mL of epichlorohydrin were added to a solution of chitosan and the pH of this mixture was adjusted to 9.0 with a well-defined amount of NaOH. After this reaction, the mixture was kept under stirring for 20 h. The pH of this mixture was adjusted to 7.0 with dilute HCl. Subsequently, the solid was filtered and washed with water and acetone [30,31]. Then, the gel was dried at 50°C to obtain the CS-ECH powder (Fig. 1c).

2.3. Characterization of the cross-linked chitosan (ECH-chitosan): attenuated total reflection–Fourier-transform infrared spectroscopy, thermal and scanning electron microscopy analysis

Attenuated total reflection–Fourier-transform infrared spectroscopy (ATR-FTIR) spectra were recorded on a Nicolet Nexus 670 (United States) equipped with a KRS-5 crystal of refractive index 2.4 and using an incidence angle of 45°. The spectra were taken in a transmittance mode in the wavenumber range of 750–4,000 cm^{-1}, with a resolution of 4 cm^{-1} and after 128 scan accumulations.

Thermogravimetric analysis was carried out using a thermogravimetric analysis TGA/SDTA 851 Mettler-Toledo instrument (TGA, Switzerland). The scanning rate about 10°C min^{-1}, from room temperature to 900°C under nitrogen atmosphere (20 mL min^{-1}) using around 5 mg of each sample.

Scanning electron microscopy images were obtained with a scanning electron microscope JEOL JSM-6400F

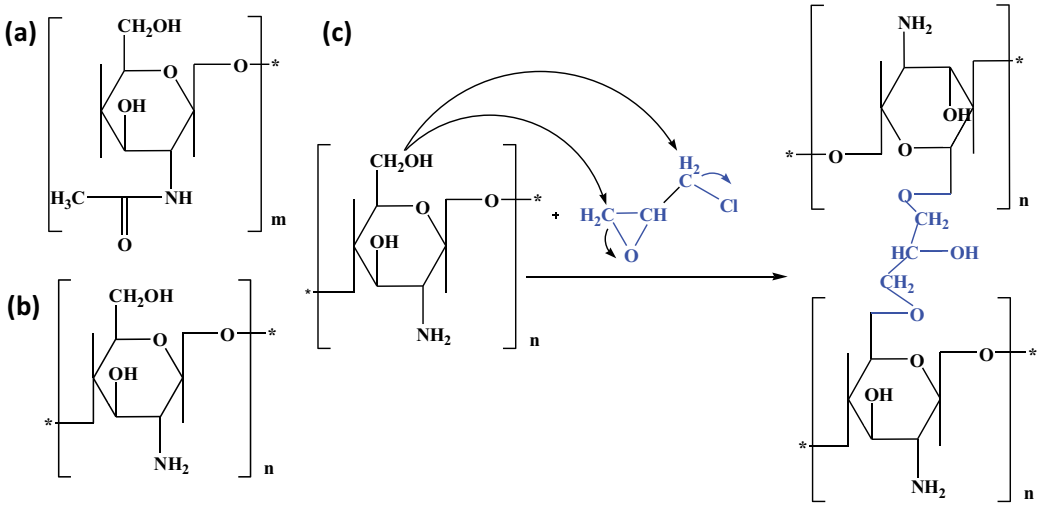

Fig. 1. Chemical structure of: chitin (a), chitosan (b), and schematic synthesis of CS-ECH (*n*: numbers of monomeric units of chitosan) (c).

(Akishima, Tokyo, Japan) with field emission cathode, a lateral resolution of 10–11 Å at 20 kV.

2.4. Congo red adsorption test and olive mill wastewater treatment

2.4.1. Adsorption experiments of Congo red

A stock solution of 1.0 g L^{-1} was prepared in distilled water. Different concentrations were obtained by successive dilutions until reaching the desired concentrations ranging from 20 to 50 mg L^{-1}. The adsorption of Congo red on chitin, chitosan and chitosan–epichlorohydrin was performed by continuous stirring for varying time in different beakers, using 0.2 g of the adsorbents with 100 mL of different Congo red concentrations. The supernatant was centrifuged for 2.0 min. Afterwards, it was filtered and analyzed by UV-Visible spectrophotometry at a wavelength of 497 nm [32]. The Congo red adsorption capacity at equilibrium (q_e) was then calculated using Eq. (1). The dye removal efficiency (R) was obtained applying Eq. (2) [33].

$$q_e = \frac{C_0 - C_e}{M} \times V \tag{1}$$

$$R = \frac{C_0 - C_e}{C_0} \times 100 \tag{2}$$

where q_e is the amount of Congo red adsorbed on the adsorbents at equilibrium (mg g^{-1}), C_0 and C_e are the initial and the equilibrium concentration of Congo red in the solution, respectively (mg L^{-1}), M denotes the weight of adsorbents (g) and V (L) represents the volume of Congo red solution.

2.4.2. Adsorption experiments of the total phenolic compounds

Fig. 2 shows the different steps of OMW treatment. The first step consists of filtering the collected olive mill wastewater. Then, the obtained solution of OMW was maintained in contact with the different adsorbents (0.3 g of the adsorbent) and was added to 10 mL of OMW. The mixture was later stirred at 300 rpm for 30 min at room temperature (22°C) using a magnetic stirrer. After centrifugation, in the resulting aqueous phase (treated OMW), the total phenolic compounds were analyzed by UV-visible spectrophotometry at 760 nm [19]. A series of gallic acid solutions (60, 120, 180, 240 and 300 mg L^{-1}) were prepared and employed to establish the calibration curve. UV-visible measurements were carried out as follows: Aliquots of gallic acid solutions (100 μL) were mixed with 6 mL of distilled water, 500 μL of Folin & Ciocalteu's Reagent and 1.5 mL of Na_2CO_3 (20% in water). These solutions were subsequently adjusted to 10 mL with distilled water and stirred vigorously after 2 h of incubation [19]. For olive mill wastewater treatment, the adsorption efficiency (%A) was calculated using Eq. (3) where C_0 and C_e are the initial and equilibrium concentrations of phenolic compounds (mg L^{-1}), respectively.

$$\%A = \frac{C_0 - C_e}{C_0} \times 100 \tag{3}$$

The regeneration of the different adsorbents was also investigated using sodium hydroxide to regenerate powder after Congo red adsorption and the acidified ethanol as eluent after OMW treatment. The samples of chitin, chitosan and chitosan–epichlorohydrin loaded Congo red (50 mg L^{-1}) after contact time (120 min) were eluted using 20 mL of sodium hydroxide. After OMW treatment, these specimens were eluted using 20 mL of acidified ethanol (ETOH-HCl) as desorbing agent [19].

2.4.3. Effect of the different parameters of the adsorption process (i e., pH, temperature, initial concentration) and isotherms of adsorption

The pH evaluation was performed as follows: a volume of 100 mL of the Congo red solution (50 mg L^{-1}) was stirred

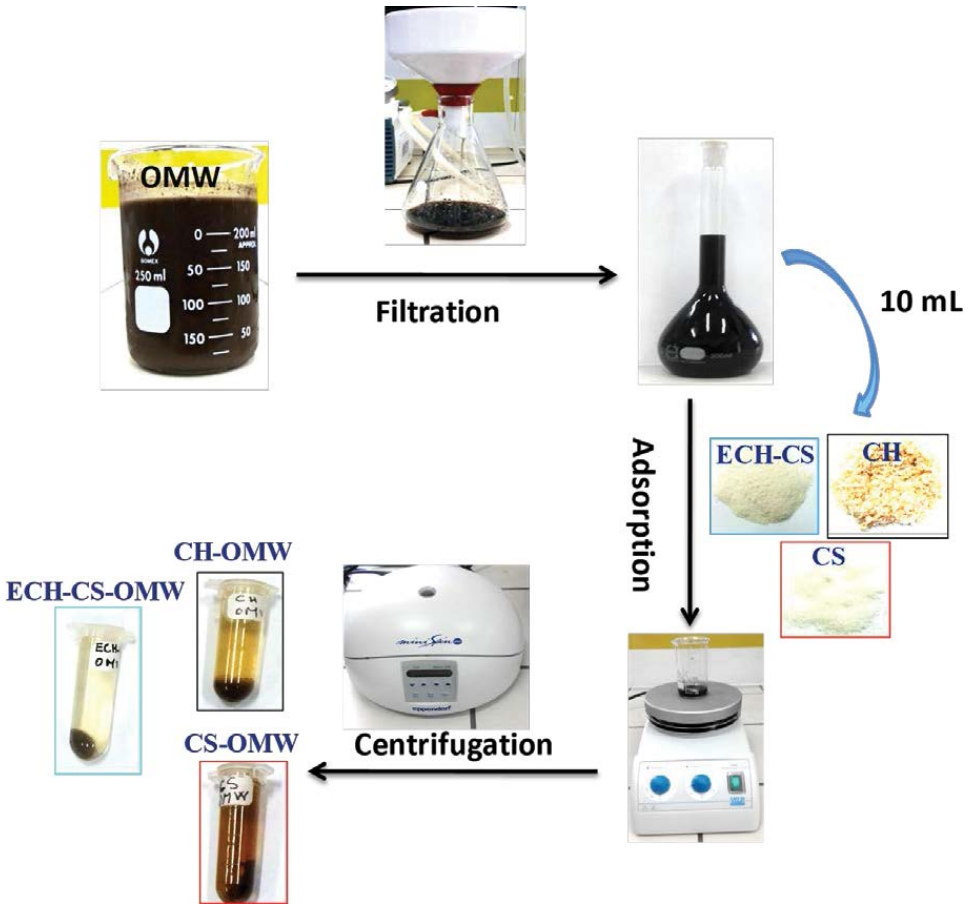

Fig. 2. Different steps of olive mill wastewater treatment (OMW) with chitin, chitosan and chitosan-ECH.

for 2 h with 0.2 g of each adsorbent. The pH of the dye solutions varied from 5 to 12 using sodium hydroxide NaOH (0.1 M) and hydrochloric acid HCl (0.1 M).

The effect of temperature on the adsorption of Congo red was studied using the same solid/liquid ratio and the same Congo red concentration for each adsorbent. The adsorption experiments were carried out without adjusting the pH and the temperature was controlled by thermometer reading.

To demonstrate the effect of dye concentration on adsorption, experiments were carried out at different dye concentrations ranging from 20 to 50 mg L^{-1}, 0.2 g of each adsorbent and each concentration of Congo red solution was stirred for a period of time equal to 120 min.

The effect of the initial mass of each adsorbent was investigated at the same pH in the Congo red solutions, at room temperature, at a constant speed and at an initial concentration of 50 mg L^{-1}. The employed adsorbent masses were 0, 0.05, 0.1 and 0.2 g.

The adsorption isotherm is the ratio between the concentration in the liquid phase and the amount of Congo red adsorbed by the adsorbents. In our study, adsorption equilibrium was achieved in concentrations ranging from 20 to 50 mg L^{-1} with a mass of 0.2 g for each material. The colored solutions were stirred with a constant stirring speed and at room temperature.

3. Results and discussion

3.1. Characterization of chitosan–epichlorohydrin

ATR-FTIR spectra of chitosan and the cross-linked chitosan (CS-ECH) are given in Fig. 3a. As displayed in this figure, the two materials presented the main FTIR bands corresponding to the vibrations of the different groups. The two ATR-FTIR spectra, showing the existence of a wide-band between 3,360 and 3,280 cm^{-1}, corresponding to the –OH and $–NH_2$ elongation vibrations. Peaks at 1,150 and 1,065 cm^{-1} can be attributed to the vibrations of elongations of C–N and C–O [30]. Two characteristic bands, related to the elongation vibrations of the $–CH_2$ and –CH groups in the epichlorohydrin, emerge at 2,920 and 2,870 cm^{-1}. The deformation vibration band appearing on the two spectra at 1,648 cm^{-1} is due to the presence of the NH of the primary amine. A vibrational elongation band for the C=O bond of the amide secondary is also observed around 1,588 cm^{-1}. The band located at 1,375 cm^{-1} is assigned to the deformation of the CH in the CH_3 group of the acetamide group present in a small proportion in the polymer chain (chitosan is not completely deacetylated) [30].

Fig. 3b shows the TGA and DTGA curves of chitosan (CS) and the cross-linked chitosan (CS-ECH). Thermogravimetric data demonstrates that the decomposition took place in the two stages of CS and CS-ECH. In the first step,

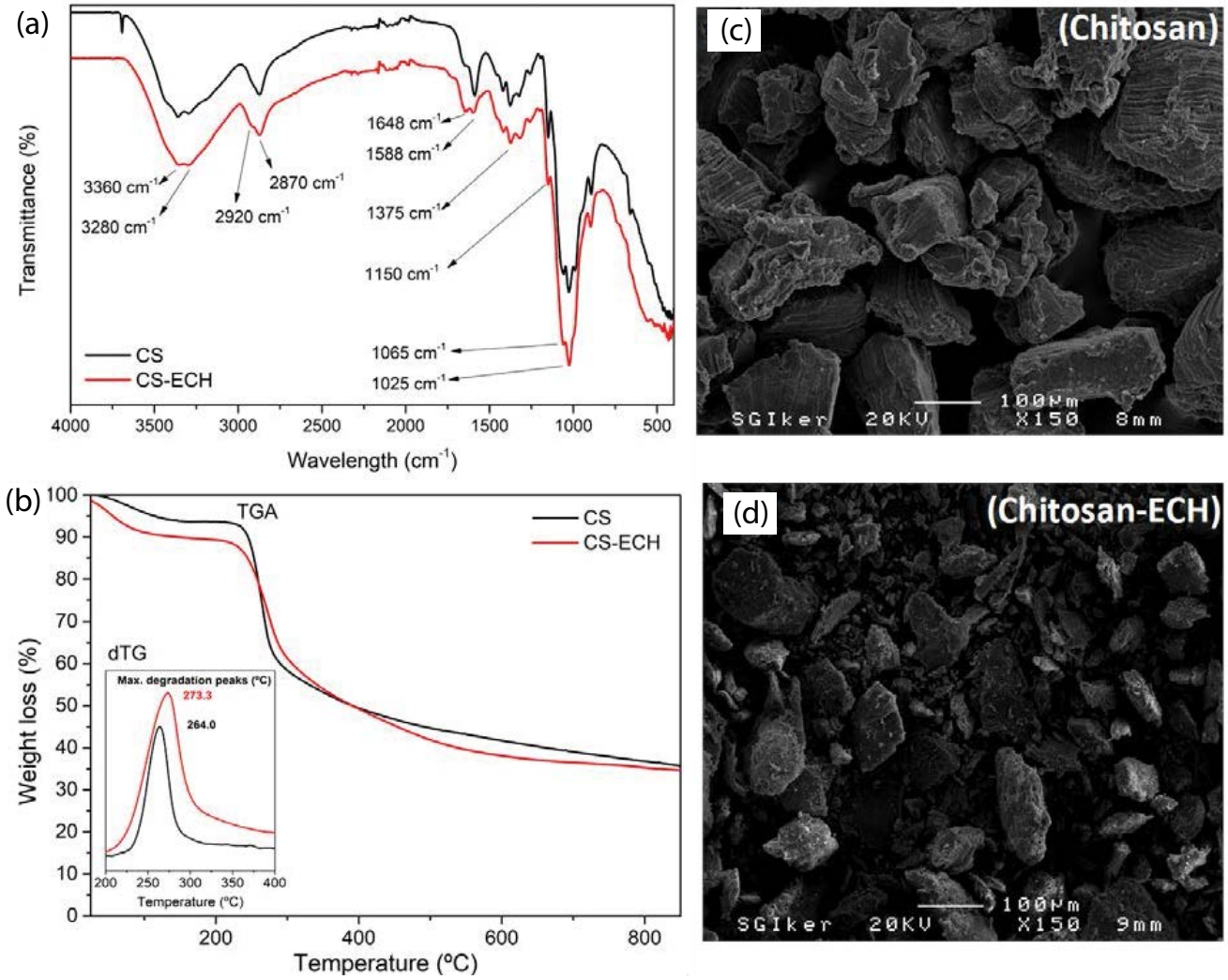

Fig. 3. ATR-FTIR spectra (a), thermal analysis (TGA and DTGA (b)) and SEM analysis (c and d) of CS and CS-ECH.

it was due to the loss of water in both polymers. The second step corresponds to the decomposition of the material itself because it is a complex process including deacetylation and depolymerization decomposition of monomeric units. The comparison of the thermograms for the two adsorbents reveals that the modified chitosan decomposes at higher temperatures, compared to pure chitosan, which shows an increase in thermal stability because of the structural modification caused by the cross-linking with epichlorohydrin.

The scanning electron microscopy (SEM) photograph of chitosan (CS) and the cross-linked chitosan (CS-ECH) are represented in Figs. 3c and d. It can be observed, from these figures, that the cross-linked chitosan has a smoother surface than chitosan. This morphological change is also in an evidence for the cross-linking of chitosan with epichlorohydrin.

3.2. Adsorption kinetics (effect of the contact time)

Figs. 4a–c depict the effect of contact time for Congo red removal by the three adsorbents (chitin, chitosan and chitosan–epichlorohydrin), respectively. Obviously, these materials show the same behavior for all the studied concentrations. This behavior is characterized, in the first minutes of adsorption, by the increase of the adsorption capacities which remains almost constant to the equilibrium time for the Congo red removal. Based on these results, it can be concluded that kinetics presents two distinct stages [34]. The fast step corresponds to the external mass transfer, while the slow stage refers to the diffusion phenomenon. In fact, the kinetics of adsorption is rapid during the first minutes of the reaction of Congo red, which can be interpreted by the fact that, at the beginning of adsorption, the number of active sites available on the surface of the adsorbents rises [35]. In addition, the increase in the initial dye concentration leads to the augmentation of the adsorption capacity resulting from the rise of the driving force of the concentration gradient which favors intraparticle diffusion [35,36]. Furthermore, an increase in the concentration gradient causes a rapid diffusion of the dye. The above-listed figures show also that the adsorption equilibrium is reached in the first 10 min for the CS-ECH with a

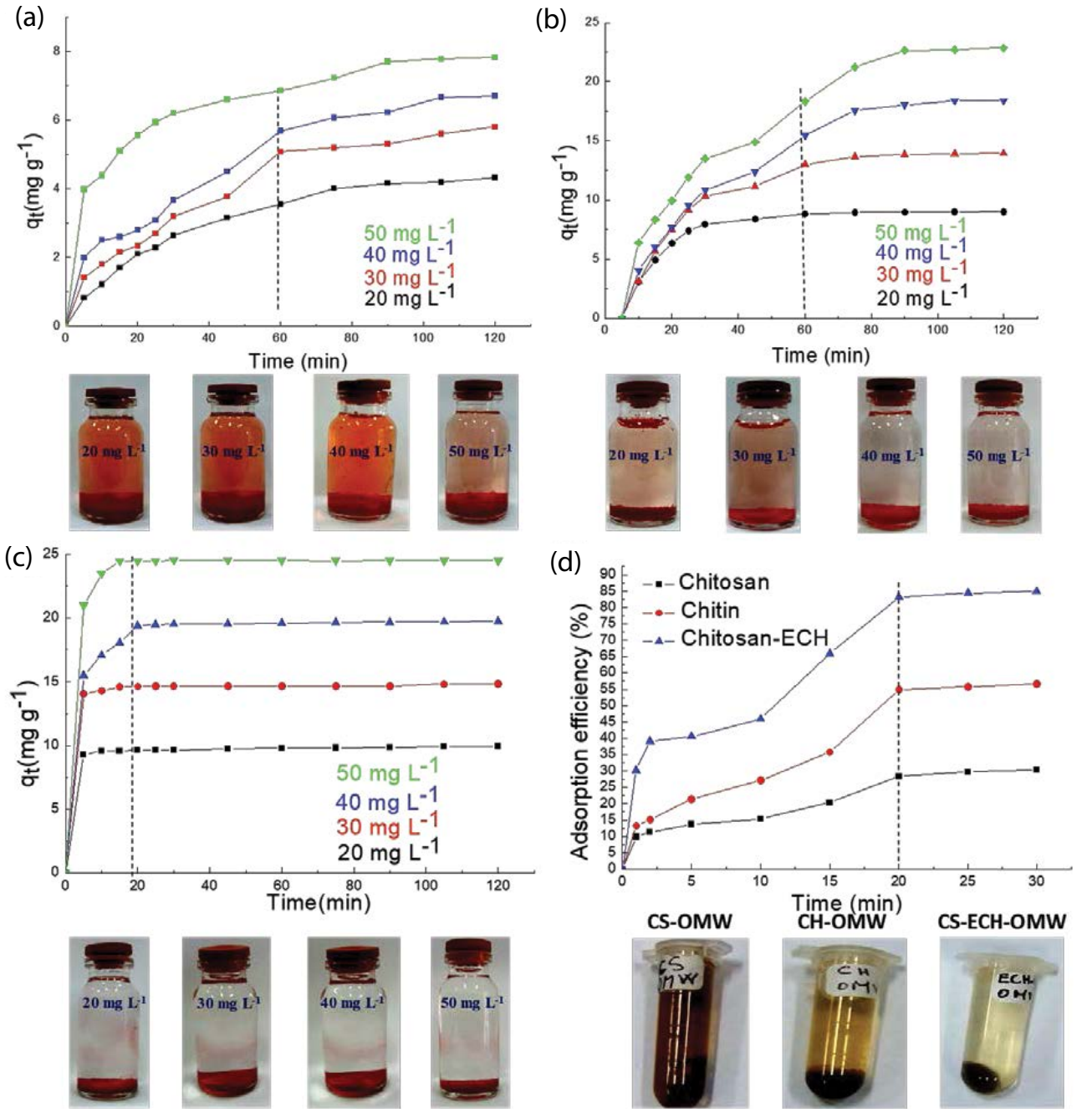

Fig. 4. Effect of contact time on the adsorption of Congo red onto CH (a), CS (b) and CS-ECH (c) at different concentrations of Congo red (20, 30, 40 and 50 mg L^{-1}) at 22°C using 0.2 g of each adsorbent; effect of contact time on the adsorption of the total phenolic compounds on CH, CS and CS-ECH (d).

high adsorption amount of 24.5 mg g^{-1} for a concentration of 50 mg L^{-1}. However, under the same concentrations of Congo red, the equilibrium time is about 60 min for chitin and chitosan. Moreover, the adsorption efficiency of the dye by CS-ECH is much greater compared to that of chitin and chitosan, while the percent of removal is 31.3%, 90.2% and 98% for CH, CS and CS-ECH respectively.

To evaluate the adsorption kinetics of Congo red (CR) by chitin, chitosan and chitosan–epichlorohydrin, three kinetic models were applied to the experimental data: The pseudo-first-order model, pseudo-second-order model and intraparticle diffusion model. The first model can be expressed as follows [Eq. (4)] [37]:

$$\log\left(q_e - q_t\right) = \log q_e - \frac{K_1}{2{,}203}t \tag{4}$$

where q_t (mg g^{-1}) is the adsorption capacity at time (t); q_e (mg g^{-1}) denotes the adsorption capacity at equilibrium and the constant K_1 (min^{-1}) designates the pseudo-first-order

kinetic model. The linear variation of the curve log ($q_e - q_t$) vs. time (t) (Figs. S1a–c) allows calculating the value of the constants K_1 and q_e for (CR) adsorption on chitin, chitosan and the cross-linked chitosan, respectively.

The equation of the model pseudo-second-order is written below [Eq. (5)] [38]:

$$\frac{t}{q_t} = \frac{1}{k_2 q_e^2} + \frac{1}{q_e} t \tag{5}$$

The plot of (t/q_t) vs. (t) permits determining the values of K_2 and q_e for (CR) adsorption on chitin, chitosan and the cross-linked chitosan, respectively. The data was then fitted to a pseudo-second-order kinetic model based on Figs. S1d–f. The kinetics parameters and the correlation coefficients are summarized in Table 1. The linear fit between the t/q_t vs. contact time (t) and the calculated correlation (R^2) > 0.99 for pseudo-second-order kinetic model show that the removal process using chitin, chitosan and chitosan–epichlorohydrin follows the pseudo-second-order kinetic model. In addition, the experimental adsorption capacity at equilibrium ($q_{e,\exp}$) values fitted well with those calculated ($q_{e,\text{cal}}$). However, the correlation coefficient (R^2) of the pseudo-first-order model is in the range of 0.9 and the calculated values ($q_{e,\text{cal}}$) and the experimental ones ($q_{e,\exp}$) are not coherent. This kinetic model cannot be employed to describe the adsorption process (Table 1) for Congo red removal by chitin, chitosan and chitosan–epichlorohydrin.

To further investigate the diffusion mechanism between Congo red and the adsorbents (CH, CS and CS-ECH), the intraparticle diffusion model (Weber–Morris model) was applied [39]. The linear equation of Weber–Morris model is expressed as follows:

$$q_t = k_p t^{1/2} + C \tag{6}$$

where k_p (mg g^{-1} min$^{-1/2}$) is the intraparticle diffusion rate constant and C (mg g^{-1}) represents a constant related to the thickness of the boundary layer. According to Eq. (6), a plot of q_t vs. $t^{1/2}$ should be a straight line with a slope k_p and intercept C when the adsorption mechanism complied with the intraparticle diffusion process. The experimental

Table 1
Parameters of the pseudo-first-order and the pseudo-second-order model for the Congo red adsorption on CH, CS and CS-ECH

Model	Materials	Parameters				
Pseudo-second-order	Chitin	C_0 (mg L^{-1})	$q_{e,\text{cal}}$ (mg g^{-1})	$q_{e,\exp}$ (mg g^{-1})	K_2 (g mg^{-1} min^{-1})	R^2
		a	5.58	4.32	0.005	0.99
		b	7.84	5.80	0.005	0.97
		c	8.48	6.70	0.007	0.96
		d	8.37	7.82	0.017	0.99
	Chitosan	*a*	9.69	9.01	0.011	0.99
		b	16.31	13.95	0.004	0.99
		c	23.25	18.42	0.002	0.98
		d	28.24	22.50	0.001	0.99
	Chitosan-ECH	*a*	9.95	9.94	0.147	0.99
		b	14.83	14.84	0.179	0.99
		c	19.92	19.75	0.048	0.99
		d	24.57	24.50	0.200	0.99
Pseudo-first-order	Chitin	C_0 (mg L^{-1})	$q_{e,\text{cal}}$ (mg g^{-1})	$q_{e,\exp}$ (mg g^{-1})	K_1 (min^{-1})	R^2
		a	4.65	4.32	0.030	0.98
		b	5.95	5.80	0.026	0.97
		c	8.55	6.70	0.034	0.87
		d	5.72	7.82	0.035	0.91
	Chitosan	*a*	5.00	9.01	0.053	0.93
		b	19.93	13.95	0.064	0.99
		c	28.76	18.42	0.052	0.94
		d	36.06	22.90	0.053	0.96
	Chitosan-ECH	*a*	0.55	9.94	0.019	0.95
		b	0.01	14.84	0.475	0.64
		c	1.72	19.75	0.033	0.77
		d	0.03	24.50	0.270	0.50

a: 20 mg L^{-1}; *b*: 30 mg L^{-1}; *c*: 40 mg L^{-1}; *d*: 50 mg L^{-1}.

results are plotted in Figs. S1g–i. As displayed in these figures, there are two separate regions for Congo red adsorption. The first straight portion was attributed to the macro-pore and micro-pore diffusion and to the instantaneous utilization of the adsorbing sites on the adsorbent's surface. However, the second region of the intraparticle diffusion model can be attributed to a very slow diffusion of the Congo red on CH, CS and CS-ECH which are the least accessible adsorption sites. This observation was due to the very slow rate of adsorbates migration from the liquid phase onto the adsorbent surface. The deviation of a straight line from the origin may be caused by the difference in the rate of mass transfer in the initial and final stages of adsorption [40]. The fitting results obtained from the slopes and intercepts of the linear portions are listed in Table 2 which shows that, for all initial concentrations, k_{p1} is higher than k_{p2} and C_2 is larger than C_1. This result indicates that the dye removal rate is higher at the beginning of the adsorption because of the large surface area of the adsorbent available for the adsorption of Congo red on CH, CS and CS-ECH [40,41].

3.3. Isotherm modeling

The Langmuir isotherm is widely used to describe the adsorption of solute from a liquid solution, based on the assumption that the adsorbed layer is a layer of one molecule on completely homogeneous surfaces, resulting in an equal amount of adsorption energies. The Langmuir model in the non-linear [Eq. (7)] and linear [Eq. (8)] forms is obtained as follows [42]:

$$q_e = \frac{K_l q_m C_e}{1 + K_l C_e} \tag{7}$$

$$\frac{c_e}{q_e} = \frac{c_e}{q_m} + \frac{1}{k_l q_m} \tag{8}$$

where q_e (mg g^{-1}) and C_e are the capacity and the amount of Congo red adsorbed at equilibrium, respectively, while q_m (mg g^{-1}) and K_l (mg L^{-1}) represent the maximum capacity and the constant adsorption Langmuir isotherm, respectively [42]. K_l and q_m can be determined from the non-linear and linear variation C_e/q_e vs. C_e for Congo red adsorption on CH, CS and CS-ECH (Figs. S2a–c). The essential characteristics of the Langmuir isotherm is expressed by a dimensionless constant called separation factor (or the equilibrium parameter), R_l, defined by Weber and Chakkravorti [43].

$$R_l = \frac{1}{1 + K_l C_0} \tag{9}$$

where C_0 (mg L^{-1}) is the initial amount of adsorbate and R_l indicates the nature of the adsorption (adsorption is favorable when the R_l value is between 0 and 1, the R_l values) for the non-linear and linear variations) (Table 3) and for the adsorption of Congo red on CH, CS and CS-ECH at different initial concentrations (20 mg L^{-1}–50 mg L^{-1}). R_l values show a favorable adsorption process of Congo red on CH, CS and CS-ECH and the R^2 correlation coefficient equal to 0.99 for both the non-linear and linear variations, which means that the Langmuir model is more efficiently applied to describe the adsorption due to the fact that the Langmuir parameters are so close for the linear and non-linear fittings [44,45].

The Freundlich model is based on the assumption that a heterogeneous surface with the participation of different sites until the adsorption energy exponentially decreases in the adsorption process [46]. The model of Freundlich in the non-linear [Eq. (10)] and linear [Eq. (11)] forms is expressed as follows:

$$q_e = K_F C_e^{\frac{1}{n}} \tag{10}$$

$$\log q_e = \frac{1}{n} \log C_e + \log K_F \tag{11}$$

where K_F (mg g^{-1}) is related to the adsorption capacity and $1/n$ represents the empirical parameter of the adsorption

Table 2
Parameters of the intraparticle diffusion model for Congo red adsorption on CH, CS and CS-ECH

Materials	C_0 (mg L^{-1})	k_{p1}	k_{p2}	C_1	C_2	R_1^2	R_2^2
Chitin	*a*	0.56	0.27	E	1.46	0.99	0.91
	b	0.51	0.40	0.18	1.47	0.96	0.82
	c	0.44	0.48	0.96	1.60	0.84	0.89
	d	0.72	0.31	2.27	4.47	0.98	0.94
Chitosan	*a*	1.67	0.07	E	8.35	0.98	0.41
	b	2.51	0.20	E	11.91	0.99	0.71
	c	2.56	0.62	E	12.12	0.99	0.72
	d	2.65	0.97	0.10	13.03	0.99	0.74
Chitosan-ECH	*a*	0.09	0.04	9.17	9.44	0.77	0.96
	b	0.19	0.04	13.70	14.32	0.86	0.73
	c	1.32	0.04	12.81	19.23	0.94	0.97
	d	0.98	0.005	19.79	24.43	0.72	0.75

E: Error; *a*: 20 mg L^{-1}; *b*: 30 mg L^{-1}; *c*: 40 mg L^{-1}; *d*: 50 mg L^{-1}.

Table 3
Linear and non-linear Langmuir and Freundlich isotherm parameters for Congo red adsorption on CH, CS and CS-ECH at 22°C

		Langmuir parameters				Freundlich parameters		
	Materials	q_m (mg g^{-1})	R_l	K_l (L mg^{-1})	R^2	K_F (mg g^{-1})	1/n	R^2
Linear form	Chitin	12.82	0.30[a]; 0.35[b]; 0.42[c]; 0.52[d]	0.04	0.98	9.97	0.52	0.96
	Chitosan	33.33	0.04[a]; 0.05[b]; 0.07[c]; 0.10[d]	0.42	0.99	9.97	0.50	0.97
	Chitosan–epichlorohydrin	34.48	0.01[a]; 0.01[b]; 0.009[c]; 0.007[d]	2.54	0.99	24.54	0.47	0.99
Non-linear form	Chitin	12.68	0.55[a]; 0.45[b]; 0.38[c]; 0.33[d]	0.04	0.98	1.24	0.51	0.98
	Chitosan	33.12	0.10[a]; 0.07[b]; 0.05[c]; 0.04[d]	0.41	0.99	10.27	0.49	0.99
	Chitosan–epichlorohydrin	33.33	0.01[a]; 0.01[b]; 0.009[c]; 0.007[d]	2.60	0.98	24.70	0.46	0.96

a: 20 mg L^{-1}; *b:* 30 mg L^{-1}; *c:* 40 mg L^{-1}; *d:* 50 mg L^{-1}.

intensity. The values of 1/n and K_F for the adsorption of Congo red on CH, CS and CS-ECH were calculated using different initial concentrations (20, 30, 40 and 50 mg L^{-1}) from the slope of the variation of the linear variation as a function of logq_e vs. C_e (Figs. S2d–f). The various parameters (non-linear and linear fitting) of the Freundlich model are summarized in Table 3. As shown in this table, the values of R^2 and K_F for the Freundlich isotherm in non-linear fitting are slightly different than those obtained in linear fitting, which indicates that the used model is unable to describe the adsorption phenomena. However, the values of 1/n are between 0 and 1, which represents favourable adsorption. The adsorption capacity of other chitosan derivatives was tested for the removal of Congo red with previous results shown in Table 4. It is clear that CS-ECH has a better percent of removal (98 %) and a maximum adsorption capacity equal to 34.48 mg/g compared to the raw chitin for the studied concentrations, chitosan utilized in our work and other adsorbents recently reported in the literature [27,47–54]. These chitosan-based materials present a good percent of removal with different chelating groups on the chitosan chain. Besides, the cross-linked chitosan (CS-ECH) used in this work for Congo red removal show high affinity toward this dye employing only the epichlorohydrin as a cross-linker.

3.4. Thermodynamics research

To assess the effect of temperature on the adsorption of Congo red and the energy variation in the adsorption process, the thermodynamic adsorption was investigated at temperatures ranging from 22°C to 42°C. The thermodynamic parameters (i.e., the enthalpy change ($\Delta H°$), the standard-free energy ($\Delta G°$) and entropy change ($\Delta S°$)) were estimated according to the nature of the adsorption process which was determined by the following equations [Eqs. (12) and (13)] [55]:

$$\Delta G° = -RT \ln K_c \tag{12}$$

$$\ln K_c = \frac{\Delta S°}{R} - \frac{\Delta H°}{RT} \tag{13}$$

Table 4
Comparison of maximum adsorption capacity of Congo red by CH, CS and CS-ECH with different adsorbent materials including CH and CS and CS-ECH synthesized in this study (in mg g^{-1})

Adsorbent materials	Adsorbents dose (mg L^{-1})	q_m (mg g^{-1})	Equilibrium time (min/h)	References
Polypyrrole/multi-walled carbon nanotubes nanocomposite	0.01	147	5 min	[47]
Magnetic chitosan–polyethylenimine	1.4	1,876	200 min	[27]
Chitosan-Fe(OH)$_3$ beads	0.2	314.45	3,000 min	[48]
Magnetic chitosan fluid	0.5	1,724	30 min	[49]
Cellulose/chitosan hydrogel beads	2.0	40	115 min	[50]
Graphene-chitosan composite hydrogel	0.015	384.62	1,440 min	[51]
Ball-milled sugarcane bagasse	10	38.2	24 h	[52]
Tea waste	0.7	23.26	12 h	[53]
Cationic surfactant-modified tea waste	0.2	106.4	12 h	[54]
Chitin	0.2	12.82	120 min	This study
Chitosan	0.2	33.33	120 min	This study
Chitosan–epichlorohydrin	0.2	34.48	120 min	This study

where (R) is the universal gas constant equal to 8.314 J mol^{-1} K^{-1} and (K_c) is the equilibrium constant. The values of ($\Delta H°$) and ($\Delta S°$) were calculated from the slope and intercept of the plot between ($\ln K_c$) vs. ($1/T$) (Figs. S3a–c). The thermodynamic parameters are summarized in Table 5. The negative values of ($\Delta G°$) at different temperatures indicate the feasibility and spontaneous nature of the Congo red adsorption on CH, CS and CS-ECH [49]. The decrease of the negative values of ($\Delta G°$) caused by the reduction of temperatures clearly shows that the adsorption was favoured at low temperatures. The negative values of ($\Delta H°$) reflect an exothermic nature of adsorption. Furthermore, the negative values of ($\Delta S°$) demonstrate the increased randomness of the solid/solution interface during the sorption of Congo red on CH, CS and CS-ECH at the internal structure of the adsorption and hence the feasibility of the process [4,55].

3.5. Effect of the variable parameters on the adsorption process of Congo red

3.5.1. Effect of pH on the adsorption

The effect of pH solution for sorption of Congo red on CH, CS and CS-ECH was investigated over a pH range of 3–12. As presented in Fig. S3d, at acidic pH, the adsorption capacities of the anionic dye by chitosan and the cross-linked chitosan are much higher than those of chitin. Chitosan and cross-linked chitosan (CS-ECH) have an amine group –NH_2, which is easily protonated in an acidic medium to give –NH_3^+. Thus, it can be concluded that the increase of the adsorption capacity of the CR at a lower pH is probably due to the increase of the electrostatic attraction between a sulfonated group (–SO_3^-) negatively charged with CR and a positively charged amine group of each adsorbent [56]. However, chitin has amide groups that cannot be easily protonated in an acid medium. Therefore, the lower electrostatic interaction between chitin and the anions leads to the decrease of the adsorption capacity of Congo red adsorbed on chitin which remains lower than that of chitosan and the cross-linked chitosan. At pH greater than 8.0, the adsorbed amount of Congo red becomes very low. Increasing the concentration of the hydroxide ions in the solution causes the deprotonation of the amino groups of the polymers, which prevents adsorption by the electrostatic repulsive force between the negatively-charged dye molecule and the adsorbents. But, an amount of quite noticeable adsorption, in this pH zone, suggests a strong implication of physical forces such as hydrogen bonding, Van der Waals force, etc. In the adsorption process [57], 3.0 was chosen as an optimum pH for the adsorption study of Congo red on all adsorbents.

3.5.2. Effect of the amount of chitin, chitosan and chitosan-ECH on Congo red adsorption

The Congo red anionic dye adsorption results obtained using CH, CS and CS-ECH powder (adsorbent dose calculated at 0 g L^{-1}–2.0 g L^{-1} dry weight) in an initial Congo red solution (50 mg L^{-1}) for 120 min, are shown in Fig. S3e. The higher adsorbent doses provide more active adsorption sites for the Congo red. A small difference of adsorption capacity is shown between 0.1 and 0.2 g due to the fact that, at a higher dose, the available CR is insufficient to cover all adsorption sites, which slightly increases the adsorption capacities [8]. The dose chosen for the adsorption studies were 0.2 g of CH, CS and CS-ECH.

3.6. Kinetic study of olive mill wastewater treatment

The concentration of the total phenols of the studied OMW sample was 8.21 g L^{-1} before adsorption [19]. 10 mL of OMW solution was stirred with 0.3 g of CH, CS and CS-ECH at room temperature (22°C) and 30 min of contact time. The adsorption efficiency (%A) of CH, CS, CS-ECH is shown in Fig. 4d. The latter demonstrates that the tested materials exhibit significant color removal, with CS-ECH being the most efficient, that is, 85% vs. 56.7% and 30.34% for CH and CS, respectively at 30 min as an equilibrium time (Fig. 4d). The foregoing data indicate that although CS-ECH shows a higher adsorption capacity for phenolic compounds, which indicates that phenolic compounds are efficiently adsorbed on CS-ECH due to the elevated number of the available sites for this adsorbent. Moreover, comparing the adsorption capacity of Congo red and the total phenols on pure CH and CS, we notice that the CS-ECH is the most performing polymeric material indicating the effect of the added functional groups on chitosan.

Table 5
Thermodynamic parameters for the adsorption of Congo red onto CH, CS and CS-ECH at an initial concentration of 50 mg L^{-1}; mass of CH, CS and CS-ECH: 0.3 g/100 mL^{-1})

Material	$\Delta H°$ (kJ mol^{-1})	$\Delta S°$ (kJ mol^{-1} K^{-1})	$\Delta G°$ (kJ mol^{-1})	T (°C)
Chitin	–22.56	–0.07	–1.91	22
			–1.21	32
			–0.51	42
Chitosan	–61.79	–0.17	–11.64	22
			–9.94	32
			–8.24	42
Chitosan–epichlorohydrin	–12.37	–0.01	–9.42	22
			–9.32	32
			–9.22	42

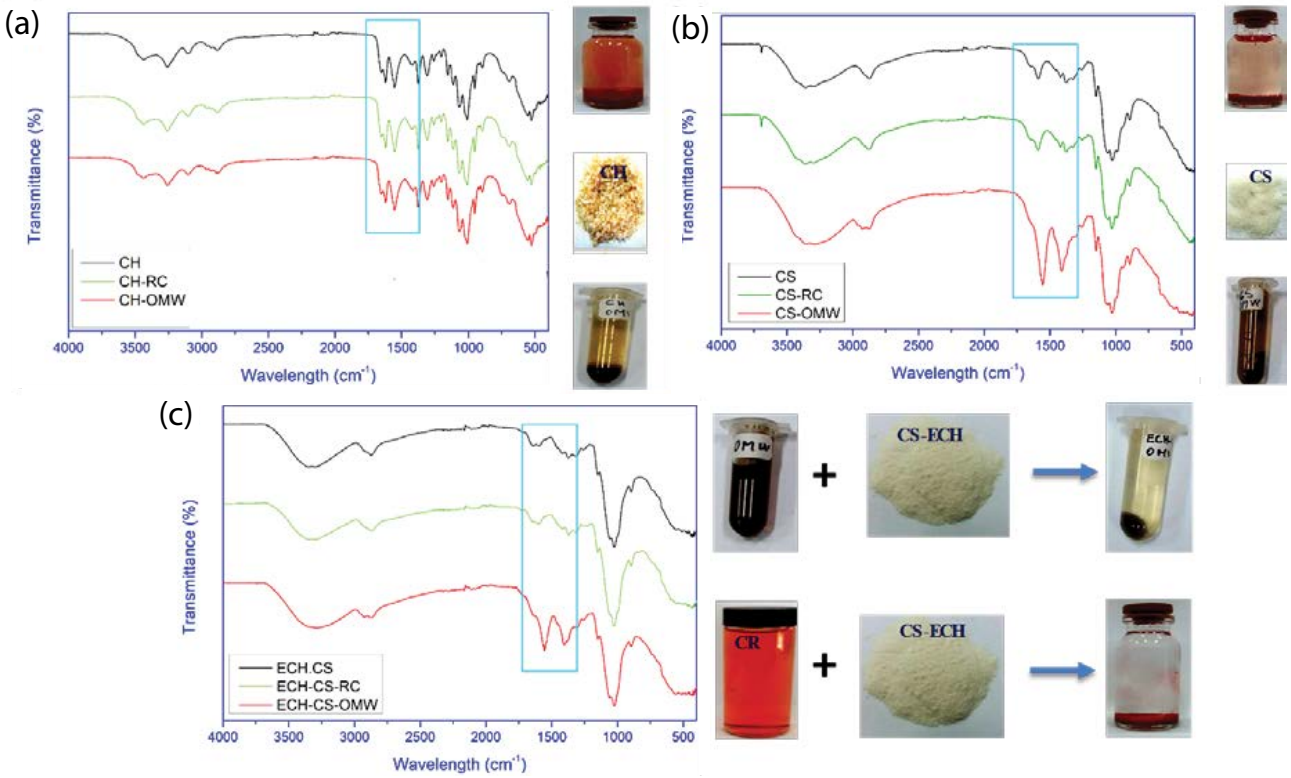

Fig. 5. ATR-FTIR spectra before and after Congo red and the total phenolic compounds adsorption on chitin (a), CS (b) and CS-ECH (c).

Consequently, CS-ECH is the more effective material for Congo red and phenolic compounds removal.

3.7. Adsorption mechanism of Congo red and phenolic compounds on CH, CS and CS-ECH

ATR-FTIR was used to determine the change in the functional groups for CH, CS and CS-ECH due to Congo red and phenolic compounds adsorption as shown in Figs. 5a–c. The ATR-FTIR spectra of the biopolymers studied before and after Congo red adsorption show no modification on the absorption bands (intensities or displacement of the wavenumbers). In fact, there is no formation of the adsorbate-adsorbent chemical bonds. The obtained experimental results prove that the mode of adsorption of Congo red on chitin, chitosan and epichlorohydrin-modified chitosan is mainly physical. The phenolic compound's adsorption on chitin is physisorption and no modification is observed in the FTIR spectra before and after adsorption. However, the FTIR spectra of chitosan and chitosan–epichlorohydrin reveal two new peaks at the wavenumbers in the range 1400 and 1540 cm^{-1}, indicating that the adsorption of the phenolic compound's on CS and CS-ECH is chemisorption [58,59]. The chemical removal of phenolic compounds by CS and CS-ECH can be explained by a new band formation between the adsorbents of the phenolic compounds in olive mill wastewater.

The SEM images of CH, CS and CS-ECH before and after Congo red and phenolic compounds uptake are represented in Fig. 6. They show a smooth surface after CR and phenolic compounds. As demonstrated, all adsorbents surfaces are visibly dissimilar to the pure adsorbents. CH, CS and especially CS-ECH display a loose and coarse surface. This result is due to the higher Congo red and phenolic compounds uptake when using CS-ECH, compared to CH and CS. A comparison of the CS-ECH and CH, CS, before and after Congo red and phenolic compounds uptake at the same magnifications, reveals a significant change in the morphologies, confirming the adsorption process. These results indicate that the surface change of CH and CS was due to the pollutants removal. However, CS-ECH shows a remarkable morphological change indicating the higher uptake of dye and phenolic compounds by CS-ECH enriched with hydroxyl (OH) and amine (NH_2) groups, which can significantly enhance its adsorption proprieties.

3.8. Desorption study

To evaluate the reusability of CH, CS and CS-ECH adsorbent, desorption experiment was conducted for Congo red and phenolic compounds. The desorption results of Congo red and the total phenols were obtained using sodium hydroxide [60,61] and ethanol-HCl [19], respectively. The desorption tests were conducted after the two pollutants removal. The different adsorbents loaded Congo red and phenolic compounds powder was eluted using the appropriate eluent and stirred for 1.0 h. Sodium hydroxide was efficiently employed to desorb the maximum amount

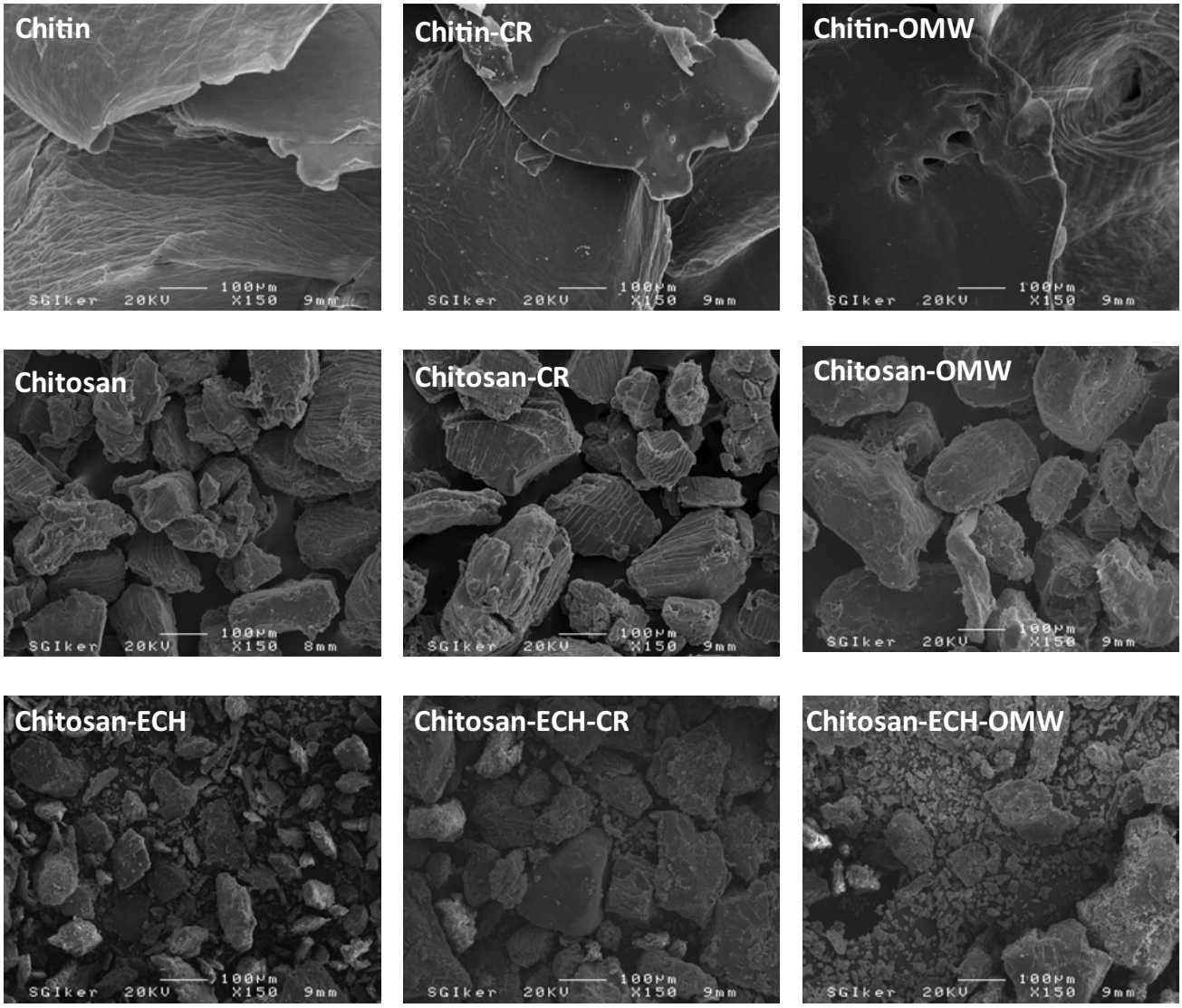

Fig. 6. SEM analysis before and after Congo red and the total phenolic compounds adsorption on chitin; CS and CS-ECH.

of Congo red from the loaded adsorbents (>51%, >53% and >61.7% for CH, CS and CS-ECH respectively for two cycles of adsorption/desorption). So, sodium hydroxide was selected as desorbing medium to desorb Congo red and regeneration of the biomaterials for further adsorption/desorption cycles. After phenolic compounds adsorption, ethanol-HCl became the appropriate eluent and it was found to be efficient for the desorption of total phenols (49%> for CS, >51% for CH and >52% for CS-ECH) up to two adsorption/desorption cycles for all adsorbents. CS-ECH derived from the chemically-modified chitosan includes hydroxyl and amine groups showing higher adsorption and desorption in the proposed condition, compared to CH and CS.

4. Conclusion

The present study showed that chitosan cross-linked with epichlorohydrin had the same potential as an adsorbent for the removal of Congo red aqueous solution and olive mill wastewater treatment. The Langmuir isotherm was found to be the suitable model for the adsorption of Congo red onto CH, CS and CS-ECH (correlation coefficient R^2 > 0.96) indicating the monolayer adsorption process. The adsorption behavior of Congo red can be well described by the pseudo-second-order model and intraparticle diffusion model associated with the adsorption process. The effects of pH, contact time, initial dye concentration and the adsorbent amount on the adsorption process of Congo red on CH, CS and CS-ECH were investigated. At pH 3.0, the adsorption of CR was highest. The thermodynamic study illustrated that the adsorption reaction for Congo red was spontaneous and exothermic in nature (the negative values of the enthalpy change and the free energy). Based on ATR-FTIR analysis before and after Congo red uptake and olive mill wastewater treatment, it was assumed that the adsorption capacity of Congo red on CH, CS and CS-ECH was augmented by physisorption. In contrast, the phenolic compound's removal by CH increased

by physisorption and chemisorption when CS and CS-ECH were used. Moreover, CH, CS and CS-ECH were regenerated after Congo red adsorption and olive mill wastewater treatment using sodium hydroxide and ethanol-HCl, respectively. The adsorbent (CS-ECH) provided a very effective and convenient tool (maximum adsorption higher than chitin and chitosan) to remove Congo red from the aqueous solution and phenolic from olive mill wastewater.

Acknowledgments

The authors wish to acknowledge the Ministry of Higher Education and Scientific Research of Tunisia and the Department of Education of the Basque Government (IT1008-16) for the financial support of this research.

Symbols and abbreviations

CH	—	Chitin
CS	—	Chitosan
CS-ECH	—	Chitosan–epichlorohydrin
CR	—	Congo red
OMW	—	Olive mill wastewater
FTIR	—	Fourier-transform infrared spectroscopy
TGA	—	Thermogravimetric analysis
DTGA	—	Differential thermogravimetric analysis
SEM	—	Scanning electron microscopy
C_0	—	Initial Congo red concentration, mg L^{-1}
C_e	—	Concentration of Congo red solution at equilibrium, mg L^{-1}
q_e	—	Amount of Congo red adsorbed at equilibrium, mg g^{-1}
q_t	—	Amount of Congo red adsorbed at time, t (mg g^{-1})
K_1	—	Constant adsorption pseudo-first-order model, min^{-1}
K_2	—	Constant adsorption pseudo-second-order model, g mg^{-1} min^{-1}
$q_{e,cal}$	—	Amount of Congo red calculated at equilibrium, mg g^{-1}
$q_{e,exp}$	—	Amount of Congo red of the experimental at equilibrium, mg g^{-1}
K_F	—	Freundlich adsorption isotherm constant, mg g^{-1}
$1/n$	—	Freundlich adsorption isotherm constant
R_l	—	Dimensionless separation constant
K_l	—	Langmuir isotherm constant related to the energy of adsorbent, L mg^{-1}
q_m	—	Maximum adsorption capacity, mg g^{-1}
T	—	Temperature, °C
Ca	—	Adsorbent phase concentration at equilibrium, mg L^{-1}
K_c	—	Equilibrium constant
$\Delta G°$	—	Standard free energy, kJ mol^{-1}
$\Delta H°$	—	Standard enthalpy change, kJ mol^{-1}
$\Delta S°$	—	Standard entropy change, kJ mol^{-1} K^{-1}

References

[1] C. Patra, R.M.N. Medisetti, K. Pakshirajan, S. Narayanasamy, Assessment of raw, acid-modified and chelated biomass for sequestration of hexavalent chromium from aqueous solution using *Sterculia villosa* Roxb. shells, Environ. Sci. Pollut. Res., 26 (2019) 23625–23637.
[2] A. Ajmani, T. Shahnaz, S. Subbiah, S. Narayanasamy, Hexavalent chromium adsorption on virgin, biochar, and chemically modified carbons prepared from *Phanera vahlii* fruit biomass: equilibrium, kinetics, and thermodynamics approach, Environ. Sci. Pollut. Res., 26 (2019) 32137–32150.
[3] C. Patra, T. Shahnaz, S. Subbiah, S. Narayanasamy, Comparative assessment of raw and acid-activated preparations of novel *Pongamia pinnata* shells for adsorption of hexavalent chromium from simulated wastewater, Environ. Sci. Pollut. Res., 27 (2020) 14836–14851.
[4] T. Shahnaz, V. Sharma, S. Subbiah, S. Narayanasamy, Multivariate optimisation of Cr(VI), Co(III) and Cu(II) adsorption onto nanobentonite incorporated nanocellulose/chitosan aerogel using response surface methodology, J. Water Process Eng., 36 (2020) 101283, https://doi.org/10.1016/j.jwpe.2020.101283.
[5] H. Zhang, Y. Ruan, Y. Feng, M. Su, Z. Diao, D. Chen, L. Hou, P. Lee, K. Shih, L. Kong, Solvent-free hydrothermal synthesis of gamma-aluminum oxide nanoparticles with selective adsorption of Congo red, J. Colloid Interface Sci., 536 (2019) 180–188.
[6] V. Karthik, K. Saravanan, C. Patra, B. Ushadevi, S. Vairam, N. Selvaraju, Biosorption of acid yellow 12 from simulated wastewater by non-viable *T. harzianum*: kinetics, isotherm and thermodynamic studies, Int. J. Environ. Sci. Technol., 16 (2019) 6895–6906.
[7] C. Lavanya, K. Soontarapa, M.S. Jyothi, R.G. Balakrishna, Environmental friendly and cost effective caramel for Congo red removal, high flux, and fouling resistance of polysulfone membranes, Sep. Purif. Technol., 211 (2019) 348–358.
[8] K. Naseem, Z.H. Farooqi, R. Begum, A. Irfan, Removal of Congo red dye from aqueous medium by its catalytic reduction using sodium borohydride in the presence of various inorganic nano-catalysts: a review, J. Cleaner Prod., 187 (2018) 296–307.
[9] U.J. Kim, S. Kimura, M. Wada, Highly enhanced adsorption of Congo red onto dialdehyde cellulose-cross-linked cellulose-chitosan foam, Carbohydr. Polym., 214 (2019) 294–302.
[10] M.A. Adebayo, J.I. Adebomi, T.O. Abe, F.I. Areo, Removal of aqueous Congo red and malachite green using ackee apple seed–bentonite composite, Colloid Interface Sci. Commun., 38 (2020) 100311, https://doi.org/10.1016/j.colcom.2020.100311.
[11] M. Hernández-Zamora, F. Martínez-Jerónimo, Congo red dye diversely affects organisms of different trophic levels: a comparative study with microalgae, cladocerans, and zebrafish embryos, Environ. Sci. Pollut. Res., 26 (2019) 11743–11755.
[12] X. Zheng, X. Li, J. Li, L. Wang, W. Jin, Y. Pei, K. Tang, Efficient removal of anionic dye (Congo red) by dialdehyde microfibrillated cellulose/chitosan composite film with significantly improved stability in dye solution, Int. J. Biol. Macromol., 107 (2018) 283–289.
[13] N.P. Khumalo, L.N. Nthunya, E. De Canck, S. Derese, A.R. Verliefde, A.T. Kuvarega, B.B. Mamba, S.D. Mhlanga, D.S. Dlamini, Congo red dye removal by direct membrane distillation using PVDF/PTFE membrane, Sep. Purif. Technol., 211 (2019) 578–586.
[14] R.E. Adam, G. Pozina, M. Willander, O. Nur, Synthesis of ZnO nanoparticles by co-precipitation method for solar driven photodegradation of Congo red dye at different pH, Photonics Nanostruct., 32 (2018) 11–18.
[15] N.P. Raval, P.U. Shah, N.K. Shah, Adsorptive amputation of hazardous azo dye Congo red from wastewater: a critical review, Environ. Sci. Pollut. Res., 23 (2016) 14810–14853.
[16] S. Dermeche, M. Nadour, C. Larroche, F. Moulti-Mati, P. Michaud, Olive mill wastes: biochemical characterizations and valorization strategies, Process Biochem., 48 (2013) 1532–1552.
[17] I. Dammak, M. Nakajima, S. Sayadi, H. Isoda, Integrated membrane process for the recovery of polyphenols from olive mill water, J. Arid. Land Stud., 25 (2015) 85–88.
[18] A. El-Abbassi, H. Kiai, A. Hafidi, Phenolic profile and antioxidant activities of olive mill wastewater, Food Chem., 132 (2012) 406–412.

[19] A. Yangui, M. Abderrabba, A. Sayari, Amine-modified mesoporous silica for quantitative adsorption and release of hydroxytyrosol and other phenolic compounds from olive mill wastewater, J. Taiwan Inst. Chem. Eng., 70 (2016) 1–8.
[20] A. El-Abbassi, H. Kiai, J. Raiti, A. Hafidi, Application of ultrafiltration for olive processing wastewaters treatment, J. Cleaner Prod., 65 (2013) 1–7.
[21] J.M. Ochando-Pulido, M.D. Víctor-Ortega, A. Martínez-Ferez, Membrane fouling insight during reverse osmosis purification of pretreated olive mill wastewater, Sep. Purif. Technol., 168 (2016) 177–187.
[22] N. Kalogerakis, M. Politi, S. Foteinis, E. Chatzisymeon, D. Mantzavinos, Recovery of antioxidants from olive mill wastewaters: a viable solution that promotes their overall sustainable management, J. Environ. Manage., 128 (2013) 749–758.
[23] A. Labidi, A.M. Salaberria, S.M.C. Fernandes, J. Labidi, M. Abderrabba, Functional chitosan derivative and chitin as decolorization materials for methylene blue and methyl orange from aqueous solution, Materials, 12 (2019) 361, doi: 10.3390/ma12030361.
[24] L. Rizzo, G. Lofrano, M. Grassi, V. Belgiorno, Pre-treatment of olive mill wastewater by chitosan coagulation and advanced oxidation processes, Sep. Purif. Technol., 63 (2008) 648–653.
[25] R. Xu, J. Mao, N. Peng, X. Luo, C. Chang, Chitin/clay microspheres with hierarchical architecture for highly efficient removal of organic dyes, Carbohydr. Polym., 188 (2018) 143–150.
[26] M. Wawrzkiewicz, P. Bartczak, T. Jesionowski, Enhanced removal of hazardous dye form aqueous solutions and real textile wastewater using bifunctional chitin/lignin biosorbent, Int. J. Biol. Macromol., 99 (2017) 754–764.
[27] L. You, C. Huang, F. Lu, A. Wang, X. Liu, Q. Zhang, Facile synthesis of high performance porous magnetic chitosan–polyethylenimine polymer composite for Congo red removal, Int. J. Biol. Macromol., 107 (2018) 1620–1628.
[28] C.Q. Ruan, M. Strømme, J. Lindh, Preparation of porous 2,3-dialdehyde cellulose beads cross-linked with chitosan and their application in adsorption of Congo red dye, Carbohydr. Polym., 181 (2018) 200–207.
[29] B. Yuan, L.G. Qiu, H.Z. Su, C.L. Cao, J.H. Jiang, Schiff base–chitosan grafted L-monoguluronic acid as a novel solid-phase adsorbent for removal of Congo red, Int. J. Biol. Macromol., 82 (2016) 355–360.
[30] Y. Yan, G. Yuvaraja, C. Liu, L. Kong, K. Guo, G.M. Reddy, G.V. Zyryanov, Removal of Pb(II) ions from aqueous media using epichlorohydrin cross-linked chitosan Schiff's base@Fe_3O_4 (ECCSB@Fe_3O_4), Int. J. Biol. Macromol., 117 (2018) 1305–1313.
[31] T.Y. Kim, S.S. Park, S.Y. Cho, Adsorption characteristics of Reactive Black 5 onto chitosan beads cross-linked with epichlorohydrin, J. Ind. Eng. Chem., 18 (2012) 1458–1464.
[32] T. Etemadinia, B. Barikbin, A. Allahresani, Removal of Congo red dye from aqueous solutions using $ZnFe_2O_4$/SiO_2/Tragacanth gum magnetic nanocomposite as a novel adsorbent, Surf. Interfaces, 14 (2019) 117–126.
[33] T. Shahnaz, V.C. Padmanaban, S. Narayanasamy, Surface modification of nanocellulose using polypyrrole for the adsorptive removal of Congo red dye and chromium in binary mixture, Int. J. Biol. Macromol., 151 (2020) 322–332.
[34] H. Hu, J. Liu, Z. Xu, L. Zhang, B. Cheng, W. Ho, Hierarchical porous Ni/Co-LDH hollow dodecahedron with excellent adsorption property for Congo red and Cr(VI) ions, Appl. Surf. Sci., 478 (2019) 981–990.
[35] L. Pietrelli, I. Francolini, A. Piozzi, Dyes adsorption from aqueous solutions by chitosan, Sep. Sci. Technol., 50 (2015) 1101–1107.
[36] J. Maity, S.K. Ray, Enhanced adsorption of methyl violet and Congo red by using semi and full IPN of polymethacrylic acid and chitosan, Carbohydr. Polym., 104 (2014) 8–16.
[37] S. Lagergren, About the theory of so–called adsorption of soluble substances, Kungliga Svenska Vetenskapsakademiens, Handlingar, 24 (1898) 1–39.
[38] Y.S. Ho, G. McKay, The kinetics of sorption of divalent metal ions onto sphagnum moss peat, Water Res., 34 (2000) 735–742.
[39] W.J. Weber, J.C. Morris, Kinetics of adsorption on carbon from solution, J. Sanit. Eng. Div., 89 (1963) 31–60.
[40] J. Ma, Y. Jia, Y. Jing, Y. Yao, J. Sun, Kinetics and thermodynamics of methylene blue adsorption by cobalt-hectorite composite, Dyes Pigm., 93 (2012) 1441–1446.
[41] A. Labidi, A.M. Salaberria, S.C.M. Fernandes, J. Labidi, M. Abderrabba, Adsorption of copper on chitin-based materials: kinetic and thermodynamic studies, J. Taiwan Inst. Chem. Eng., 65 (2016) 140–148.
[42] I. Langmuir, The adsorption of gases on plane surfaces of glass, mica and platinum, J. Am. Chem. Soc., 40 (1918) 1361–1403.
[43] T.W. Weber, R.K. Chakkravorti, Pore and solid diffusion models for fixed-bed adsorbers, AIChE J., 20 (1974) 228–238.
[44] J.K. Sahoo, S.K. Paikra, M. Mishra, H. Sahoo, Amine functionalized magnetic iron oxide nanoparticles: synthesis, antibacterial activity and rapid removal of Congo red dye, J. Mol. Liq., 282 (2019) 428–440.
[45] K.C. Nebaghe, Y. El Boundati, K. Ziat, A. Naji, L. Rghioui, M. Saidi, Comparison of linear and non-linear method for determination of optimum equilibrium isotherm for adsorption of copper(II) onto treated Martil sand, Fluid Phase Equilib., 430 (2016) 188–194.
[46] H.M. Freundlich, Over the adsorption in solution, J. Phys. Chem., 57 (1906) 385–471.
[47] R.S. Aliabadi, N.O. Mahmoodi, Synthesis and characterization of polypyrrole, polyaniline nanoparticles and their nanocomposite for removal of azo dyes; sunset yellow and Congo red, J. Cleaner Prod., 179 (2018) 235–245.
[48] Y. Li, H. Gao, C. Wang, X. Zhang, H. Zhou, One-step fabrication of chitosan-$Fe(OH)_3$ beads for efficient adsorption of anionic dyes, Int. J. Biol. Macromol., 117 (2018) 30–41.
[49] M. Hui, P. Shengyan, H. Yaqi, Z. Rongxin, Z. Anatoly, C. Wei, A highly efficient magnetic chitosan "fluid" adsorbent with a high capacity and fast adsorption kinetics for dyeing wastewater purification, Chem. Eng. J., 345 (2018) 556–565.
[50] M. Li, Z. Wang, B. Li, Adsorption behaviour of Congo red by cellulose/chitosan hydrogel beads regenerated from ionic liquid, Desal. Water Treat., 57 (2016) 16970–16980.
[51] S. Omidi, A. Kakanejadifard, Eco-friendly synthesis of graphene–chitosan composite hydrogel as efficient adsorbent for Congo red, RSC Adv., 8 (2018) 12179–12189.
[52] Z. Zhang, L. Moghaddam, I.M. O'Hara, W.O. Doherty, Congo red adsorption by ball-milled sugarcane bagasse, Chem. Eng. J., 178 (2011) 122–128.
[53] M. Foroughi-Dahr, H. Abolghasemi, M. Esmaili, A. Shojamoradi, H. Fatoorehchi, Adsorption characteristics of Congo red from aqueous solution onto tea waste, Chem. Eng. Commun., 202 (2015) 181–193.
[54] M. Foroughi-dahr, H. Abolghasemi, M. Esmaieli, G. Nazari, B. Rasem, Experimental study on the adsorptive behavior of Congo red in cationic surfactant-modified tea waste, Process Saf. Environ. Prot., 95 (2015) 226–236.
[55] M. Chahkandi, Mechanism of Congo red adsorption on new sol–gel-derived hydroxyapatite nano-particle, Mater. Chem. Phys., 202 (2017) 340–351.
[56] A. Zahir, Z. Aslam, M.S. Kamal, W. Ahmad, A. Abbas, R.A. Shawabkeh, Development of novel cross-linked chitosan for the removal of anionic Congo red dye, J. Mol. Liq., 244 (2017) 211–218.
[57] L. Meng, X. Zhang, Y. Tang, K. Su, J. Kong, Hierarchically porous silicon–carbon–nitrogen hybrid materials towards highly efficient and selective adsorption of organic dyes, Sci. Rep., 5 (2015) 7910, doi: 10.1038/srep07910.
[58] M. Masmoudi, C. Rahal, R. Abdelhedi, M. Khitouni, M. Bouaziz, Inhibitive action of stored olive mill wastewater (OMW) on the corrosion of copper in a NaCl solution, RSC Adv., 5 (2015) 101768–101775.

[59] M. Achak, A. Hafidi, L. Mandi, N. Ouazzani, Removal of phenolic compounds from olive mill wastewater by adsorption onto wheat bran, Desal. Water Treat., 52 (2014) 2875–2885.
[60] A. Sharma, Z.M. Siddiqui, S. Dhar, P. Mehta, D. Pathania, Adsorptive removal of Congo red dye (CR) from aqueous solution by *Cornulaca monacantha* stem and biomass-based activated carbon: isotherm, kinetics and thermodynamics, Sep. Sci. Technol., 54 (2018) 916–929.
[61] V.S. Munagapati, D.S. Kim, Equilibrium isotherms, kinetics, and thermodynamics studies for Congo red adsorption using calcium alginate beads impregnated with nano-goethite, Ecotoxicol. Environ. Saf., 141 (2017) 226–234.

Supporting information

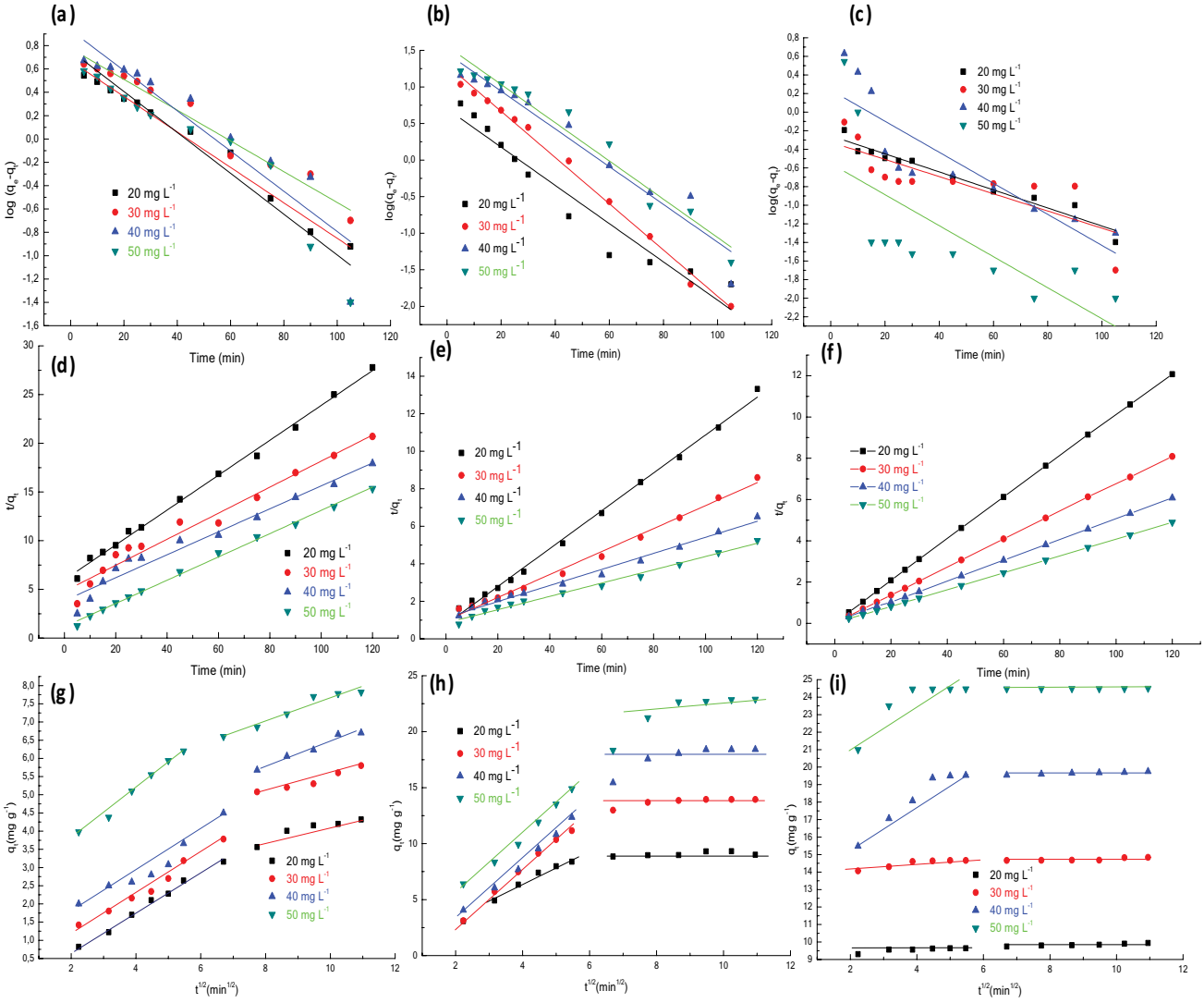

Fig. S1. Pseudo-first-order (CH (a), CS (b) and CS-ECH (c)), pseudo-second-order (CH (d), CS (e) and CS-ECH (f)), intraparticle diffusion model (CH (g), CS (h) and CS-ECH (i)) for Congo red adsorption onto CH, CS and CS-ECH.

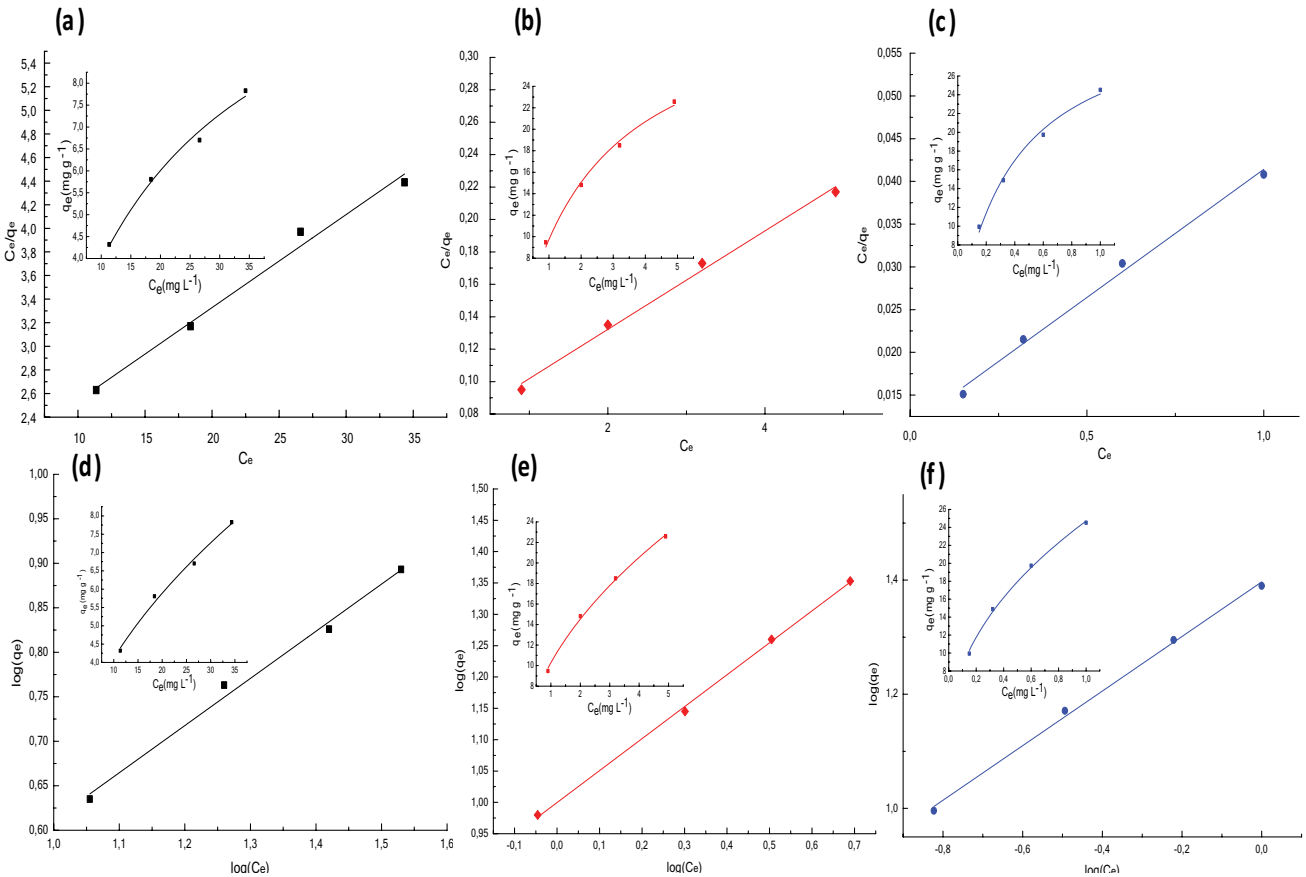

Fig. S2. Linear and non-linear Langmuir (CH (a), CS (b) and CS-ECH (c)), linear non-linear Freundlich (CH (d), CS (e) and CS-ECH (f)) plots for adsorption of Congo red. Conditions: 0.2 g/100 mL^{-1}; dose of adsorbent at 22°C.

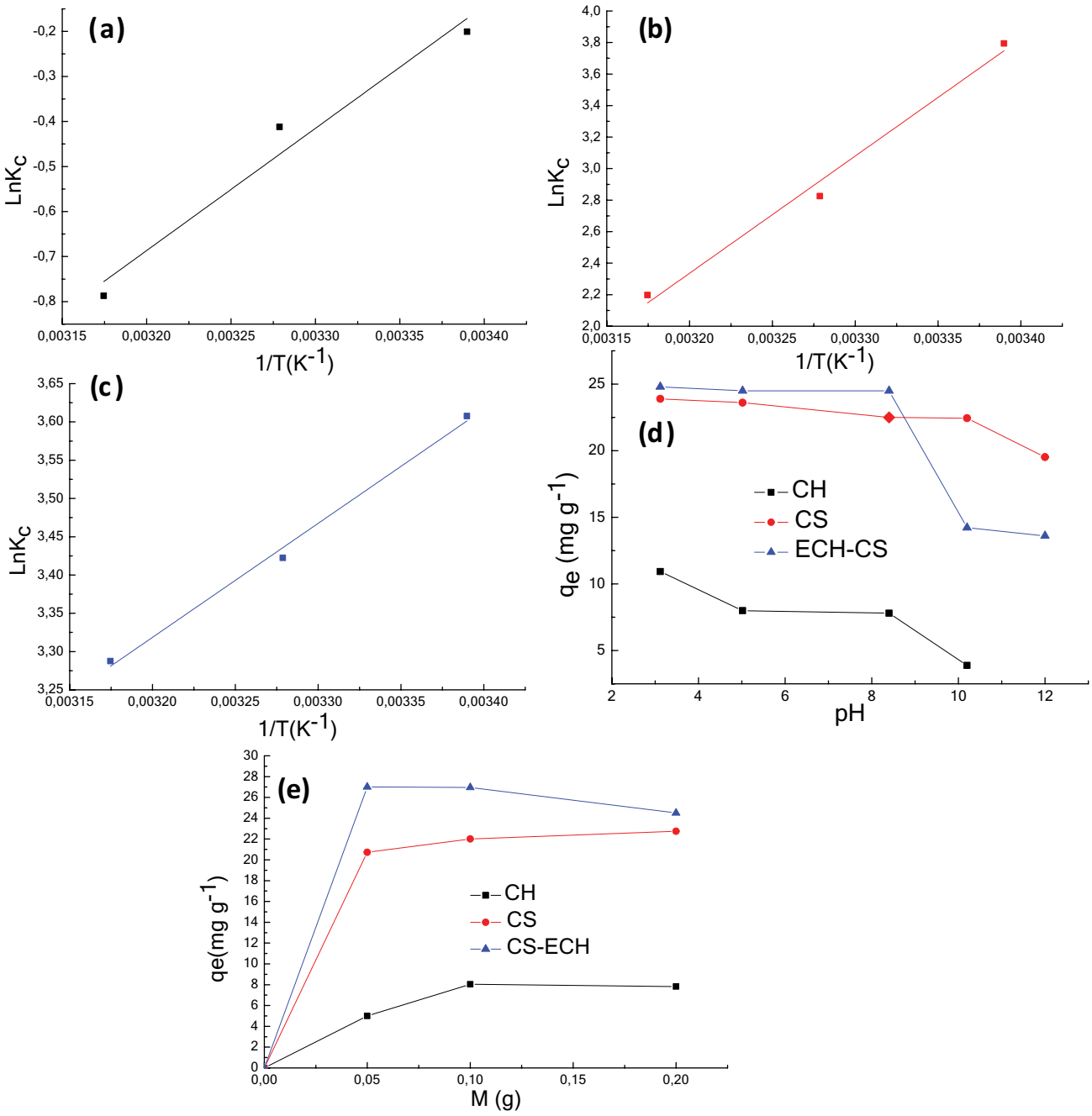

Fig. S3. Plot of lnK_c vs. 1/T for the determination of enthalpy and entropy changes (CH (a), CS (B) and CS-ECH (C)), effect of the pH (d), the mass of the adsorbent (e) on the adsorption of Congo red onto CH, CS and CS-ECH. Under the following conditions: reaction time = 120 min; dye concentration = 50 mg L^{-1}; V = 100 mL; stirring speed = 300 rpm.